

Supplementary Information: Proton Conduction Mechanisms in Phosphoric Acid at Various Water Contents: A ^1H , ^{31}P and ^{17}O PFG-NMR and Conductivity Study of the System $\text{H}_4\text{P}_2\text{O}_7 - \text{H}_3\text{PO}_4 -$ $\text{H}_3\text{PO}_4 \cdot 2\text{H}_2\text{O}$

Jan-Patrick Melchior, Klaus-Dieter Kreuer and Joachim Maier

October 21, 2016

1 Experimental

Humidifier A humidifier system was used to set water contents between $\text{P}_2\text{O}_5 \cdot 2.5\text{H}_2\text{O}$ and $\text{P}_2\text{O}_5 \cdot 3.1\text{H}_2\text{O}$ for NMR measurement. Inside the humidifier a constant N_2 gas flow is led through water in a temperature controlled vessel (see figure 1) to ensure saturation of the gas. The water saturated gas is then led to the *sample chamber*, containing the sample in a Teflon container with inside thread. Spatial separation of humidifier and sample chamber by the temperature controlled *transfer zone* ensures independent temperature control in the two compartments. With the temperature (in Celsius) in both humidifier T_W and sample chamber T_S the saturation partial water pressure in the respective compartments e_W and e_S are calculated according to the empirical equations:

$$\begin{aligned} e_{W,S}(T_{W,S}(^{\circ}\text{C})) &= 6.1078 \cdot 10^{7.5 \cdot T_i / (237.3 + T_i)} \text{ hPa}; & T < 70^{\circ}\text{C} \\ e_{W,S}(T_{W,S}(^{\circ}\text{C})) &= 5.94062 \cdot 10^{7.28829 \cdot T_i / (226.531 + T_i)} \text{ hPa}; & T > 70^{\circ}\text{C} \end{aligned} \quad (1)$$

obtained from a fit to literature data.[1] The relative humidity (*RH*) is calculated from the ratio of saturation water pressure in both chambers:

$$RH = \frac{e_W}{e_S} \cdot 100\% \quad (2)$$

The sample container can be closed without opening the humidifier through a hole in the sample chamber's top lid. This hole is sealed by the sample containers upper part (a Teflon rod with outside thread) while the sample equilibrates. The relation between *RH* and water uptake is known from TGA measurements (see figure 2 main text) and have been checked for consistency between the two setups. For $\text{P}_2\text{O}_5 \cdot 3\text{H}_2\text{O}$ (i.e. nominally dry sample) the water content after equilibration in the humidifier was evaluated by ^{31}P -NMR and compared to nominally dry freshly fused crystalline H_3PO_4 (see sample preparation).

Impedance Cell Impedance spectroscopy experiments are conducted in a pseudo-four-point setting in a T-shaped Duran glass cell (figure 2) with two circular platinum electrodes. The sample chamber ($V \sim 3\text{ml}$) is filled through a central tapping socket which is sealed gas tight during the temperature dependent measurement by a glass insert containing a type K thermocouple through which temperature is controlled. Temperatures above $T = 60^{\circ}\text{C}$ have been set in a Memmert ULE 400 oven and temperatures below $T = 60^{\circ}\text{C}$ in a Lauda RE207 thermostat.

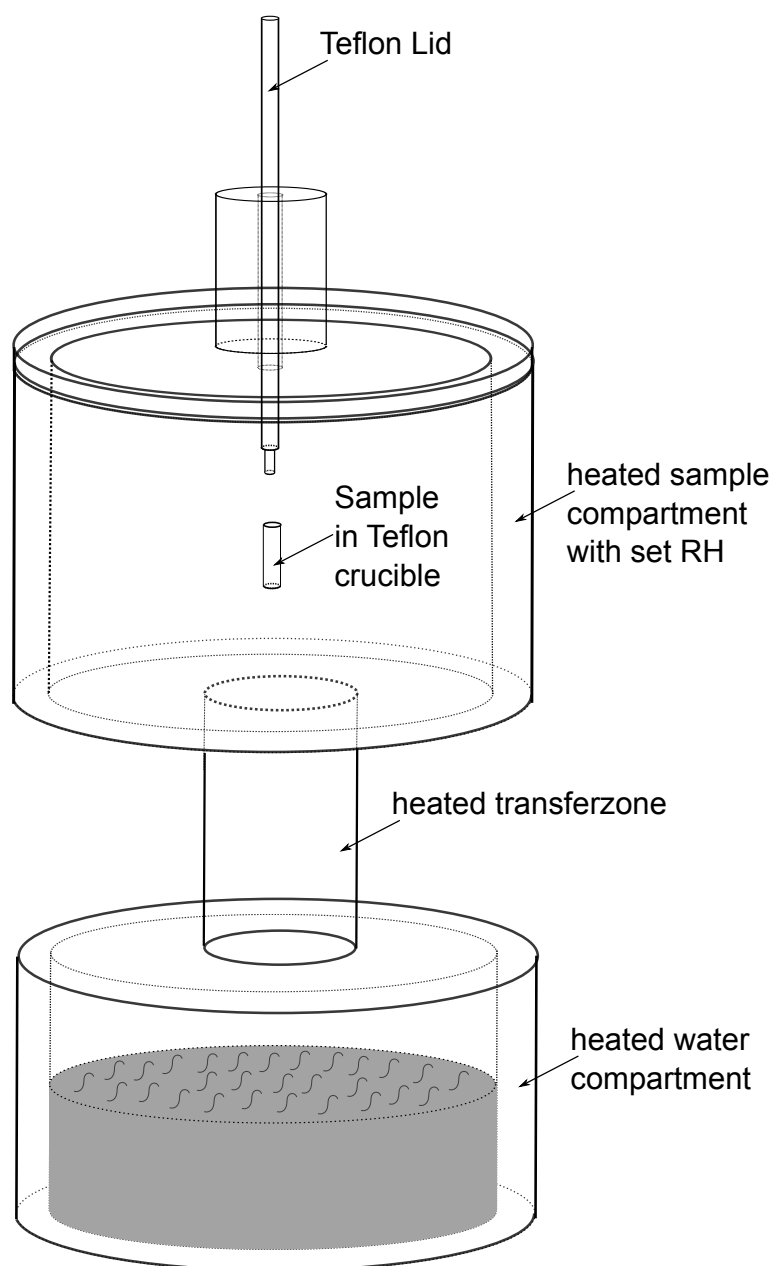


Figure 1: Schematic of the humidifier system consisting of independently temperature controlled water compartment, transferzone and sample chamber. A Teflon NMR sample holder can be inserted and manipulated through the closed sample chamber lid.

Equilibrium at low water contents The multitude of condensation and dissociation equilibria in phosphoric acid make extended equilibration times necessary. For neat phosphoric acid complete compositional equilibrium is reached after weeks at its melting point.[2] This estimate has been confirmed by measuring the ^{17}O exchange between H_2O and H_3PO_4 which takes place through condensation reactions. For lower water contents even longer equilibration times can be expected and equilibrium compositions of higher temperatures are “frozen in”

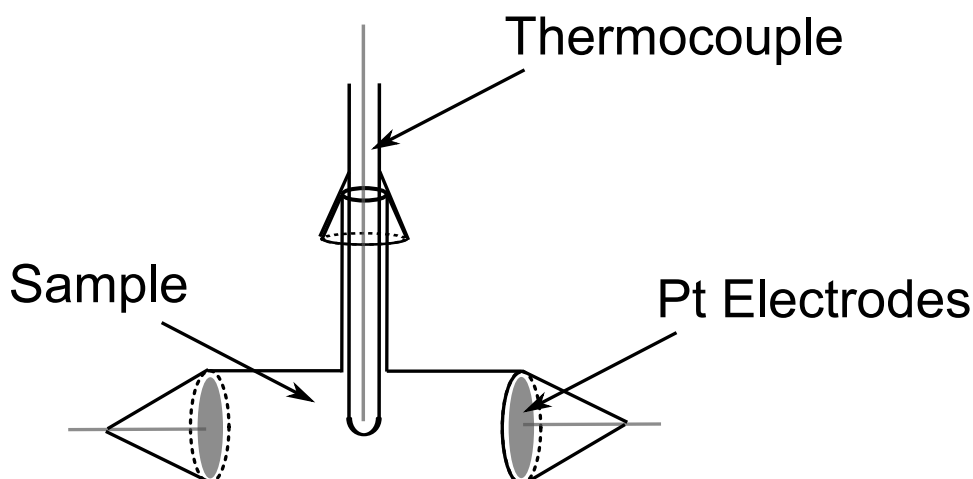


Figure 2: Schematic of the T-shaped impedance cell including a type K thermocouple and Pt electrodes to either side.

by fast cooling of the sample. As already pointed out by Munson in 1964 this might be the reason for the severe difference between compositional data for neat H_3PO_4 obtained by Munson [2] ($\sim 2\%\text{H}_2\text{O}$) and by Huhiti et. al.[3] and Jameson[4] ($\sim 6\%\text{H}_2\text{O}$). In this work compositions have therefore only be analyzed by ^{31}P -NMR at elevated temperatures ($T > 70^\circ\text{C}$). Extrapolation towards lower temperatures reproduces the data of Munson. On the other hand, stable conductivity, diffusion and T_1 relaxation times are reached at much lower equilibration times and despite non-equilibrium compositions.

^{17}O -NMR The low natural abundance ($>0.038\%$) of ^{17}O and its low (quadrupolar) relaxation rates make ^{17}O PFG-NMR challenging. Enriched water (10 %) was used to prepare samples in the range $4 < \lambda < 8$. Due to oxygen the hydrolysis-condensation equilibrium reaction with pyrophosphoric acid oxygen exchanges between H_3PO_4 and H_2O . In freshly mixed samples a clear shift of intensity from the H_2O peak to the H_3PO_4 peak (see figure 3). To ensure full equilibration, samples have been kept in sealed NMR tubes at increased temperature for

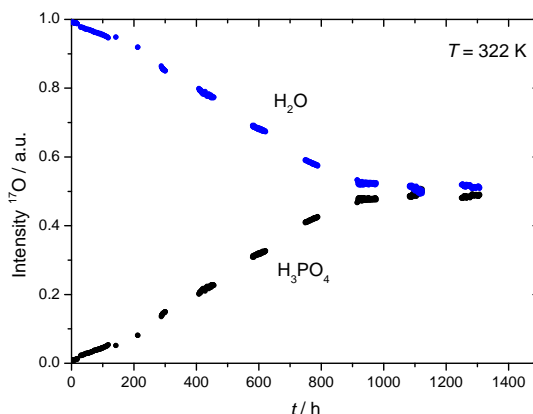


Figure 3: Relative peak intensity of H_2O and H_3PO_4 in ^{17}O NMR experiment over time. Samples was prepared by mixing 10% ^{17}O enriched water with crystalline nominally dry H_3PO_4 . Sample was kept at $T = 322\text{ K}$ for roughly 2 month.

up to several weeks till homogenous distribution of ^{17}O between H_3PO_4 and H_2O was reached and no changes

in the ^{17}O NMR spectrum over time could be seen. Due to the low relaxation times we use relatively low levels of enrichment and can only measure at elevated temperatures ($>370\text{ K}$) with low diffusion times ($<4\text{ ms}$) and the PFGSE sequence. The maximum gradient strength for the experiments did not exceed 20 T/m . The number of accumulations necessary for is quite high and the experiments are therefore time consuming despite low remagnetization times.

Transference experiment Literature transference measurements for phosphoric acid in aqueous solution conducted by diverse methods in the 1950's and 1960's [5–7] are only available for dilute aqueous solutions (highest concentration $56\text{ wt}\%$). Those works only distinguish between positive and negative charge being transferred. In this work we distinguish between transport by structural diffusion and vehicle conductivity (positive and negative ionic charge carrier transport) at low water contents.

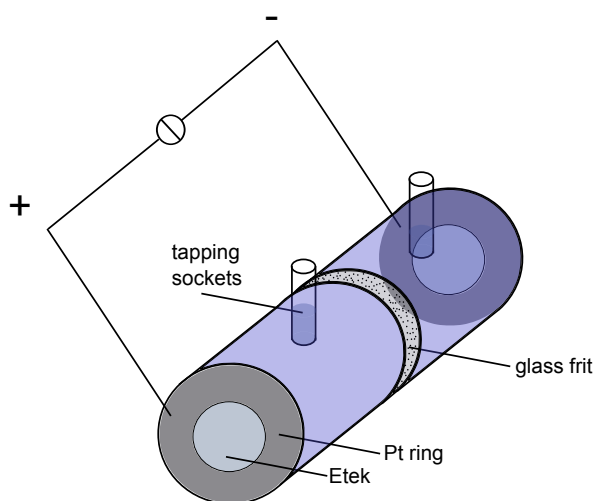


Figure 4: Schematic of the transference cell.



Figure 5: Picture of the transference cell. The electrodes are housed in an inner Teflon ring (white) and an outer PVC ring (red) used to press the electrodes against the glass container.

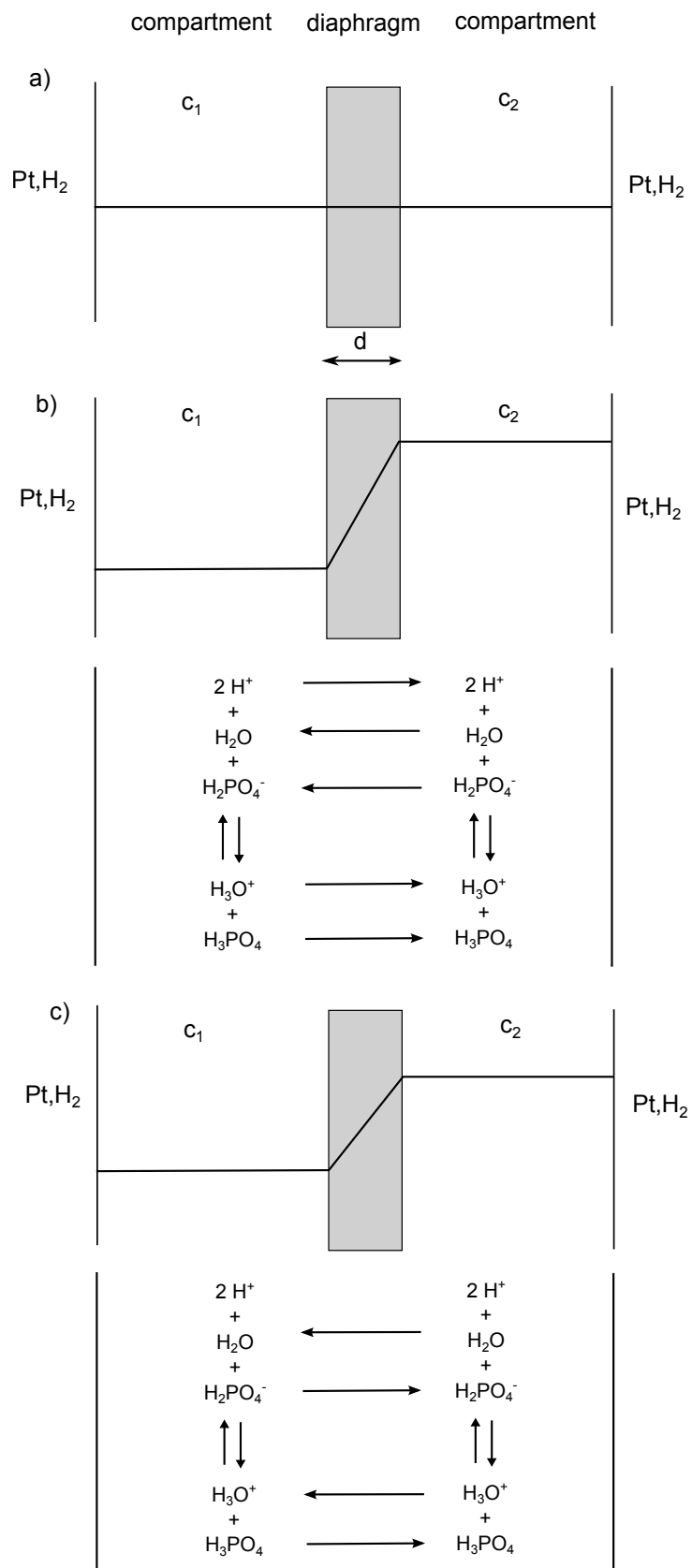


Figure 6: Concentration gradient and particle flux a) at $t=0$, b) at the stationary state and c) after turning of the current (relaxation). Homogeneous concentration in the compartments and a linear concentration gradient in the diaphragm are assumed in all cases, i.e. particle flux is the flux through the diaphragm.

The transference measurement was conducted at $T = 60^\circ\text{C}$ in a glass cell (see figure 4) consisting of an anode and cathode compartment separated by a ceramic diaphragm (pore size $10 - 16\ \mu\text{m}$), each compartment containing a hydrogen (5% H_2 in Ar) breathing hydrophobic gas diffusion electrode ($A = 6.15\ \text{cm}^2$) as commonly used in PEM fuel cells. Both compartments ($V = 8.3\text{ml}$) were filled with a phosphoric acid - water solution of identical composition and the transference cell was placed inside a desiccator with humidified gas. Experiments were conducted for $\lambda = 4.92$ (85wt% H_3PO_4 (aq)) and $\lambda = 7$ (73wt% H_3PO_4 (aq)) with humidified stream corresponding to the water partial pressure of 85wt% H_3PO_4 or 73wt% H_3PO_4 (aq) at $T = 60^\circ\text{C}$, respectively.[8] For this purpose gas stream was fed through a bubbler containing 85wt% H_3PO_4 or saturated MgCl_2 (aq).[9]

A current $I_{outer} = 30\text{mA}$ was applied and samples of volume 0.3 ml were extracted a different times t from both compartments with a syringe through tapping sockets. As concentrations in each compartment are homogenized through convection and changes of the concentration in the compartments occur as a result of H_2O -, H_3PO_4 -, H_3O^+ -, H_2PO_4^- flux through the diaphragm (thickness $d = 2.5\ \text{mm}$, see below) water concentrations in the extracted sample at different times allow to analyze that particle flux. The concentrations were analyzed by ^{31}P -NMR conducted in a Bruker Avance Spectrometer at a magnetic field strength of 7.05 T and in Wilmad double walled NMR tubes. Phosphoric acid samples were contained in the outer compartment, while D_2O served as standard for deuterium lock in the inner compartment. Comparison of respective phosphorous chemical shifts with a reference curve of chemical shift values versus water content (see figure 5 main text) allows for accurate analysis of the small sample volumes. The loss of electrolyte volume in the compartments through the extraction was included in the calculation of $\lambda_1(t)$ and $\lambda_2(t)$ and the t values in figure 12 of the main text have been calculated as to correspond to a constant volume of 8.3 ml in both compartments. To express the concentration difference $\Delta\lambda(t)$ in relation to the particle flux the molar ratio λ is expressed as a volume concentration difference

$$\Delta c = \left[\frac{98 \frac{\text{g}}{\text{mol}} \cdot 2}{\lambda_1 - 3} + 18 \frac{\text{g}}{\text{mol}} \right]^{-1} \cdot \rho_1 - \left[\frac{98 \frac{\text{g}}{\text{mol}} \cdot 2}{\lambda_2 - 3} + 18 \frac{\text{g}}{\text{mol}} \right]^{-1} \cdot \rho_2 \quad (3)$$

with the respective density ρ (see figure 11) at $T = 60^\circ\text{C}$. Data shown in the main text and in figure 7 and 9 include points of two separate reproducible runs of the transference experiment.

At the beginning of the experiment the water concentration c_1 and c_2 in both compartment is equal ($\Delta c(t=0) = 0$, figure 6a). For i_x indicating charge flux, j_x particle flux and F being Faraday's constant under applied current ($I_{outer} = 30\text{mA}$) the water concentration gradient between the two compartment does not change through structural conductivity of protons $\frac{1}{F}i_{structural} = j_{\text{H}^+}$, but increases through H_3O^+ and H_2PO_4^- vehicle conductivity associated with the particle flux $\frac{1}{F}i_{veh} = j_{\text{H}_3\text{O}^+} + j_{\text{H}_2\text{PO}_4^-}$. Concentrations are homogeneous inside the compartments and the concentration difference build up through particle transport is assumed to decay with a linear gradient over the thickness of the diaphragm.

The different current contribution/ conductivity contributions of vehicle and structural conductivity are assessed by transference numbers $t_{veh} + t_{structural} = 1$ with $i_{veh} = t_{veh}I_{outer}$ and $i_{structural} = t_{structural}I_{outer}$ (see main text for conductivity contributions and transference numbers). The entities i_{veh} and t_{veh} can be measured through analysis of the time evolution of Δc as applied current, or $i_{veh} = t_{veh}I_{outer}$ to be precise, directly leads to a build up of Δc

$$\frac{\partial}{\partial t} \Delta c = -\text{div} \left(\frac{1}{F} i_{veh} \right). \quad (4)$$

However, with increasing Δc the concentration gradient causes a flux $j_{\text{H}_2\text{O}}$ opposite the flux of H_3O^+ and a flux $j_{\text{H}_3\text{PO}_4}$ opposite the flux of H_2PO_4^- (figure 6 b).

The different fluxes just compensate at the steady state for which $\Delta c(t) = \Delta c_{steady} = \text{const.}$ However, as the transported ions and neutral species interchange



at the steady state it is therefore:

$$j_{\text{H}_2\text{O}} \neq -\frac{1}{F} i_{\text{H}_3\text{O}^+} \quad (7)$$

$$j_{\text{H}_3\text{PO}_4} \neq -\frac{1}{F} i_{\text{H}_2\text{PO}_4^-}. \quad (8)$$

Instead of separate flow of the existing species the net flow of all aqueous species (H_2O and H_3O^+) $j_{aq}(= \frac{1}{F}i_{aq})$ and the net flow of all phosphoric acid species (H_3PO_4 and H_2PO_4^-) $j_{P1}(= \frac{1}{F}i_{P1})$ need to be considered. In the steady state it is therefore

$$\frac{1}{F}i_{aq} = j_{\text{H}_3\text{O}^+} + j_{\text{H}_2\text{O}} = 0 \quad (9)$$

$$-\frac{1}{F}i_{P1} = j_{\text{H}_2\text{PO}_4^-} + j_{\text{H}_3\text{PO}_4} = 0. \quad (10)$$

with

$$i_{ges} = \underbrace{i_{aq} + i_{P1}}_{i_{veh}} + \underbrace{i_{\text{H}^+}}_{i_{struc}} \quad (11)$$

$$= F \left(\underbrace{j_{\text{H}_3\text{O}^+} + j_{\text{H}_2\text{O}} - j_{\text{H}_2\text{PO}_4^-} - j_{\text{H}_3\text{PO}_4}}_{j_{veh}} + \underbrace{j_{\text{H}^+}}_{j_{struc}} \right). \quad (12)$$

linking the transport of H_3PO_4 , H_2O , H_2PO_4^- and H_3O^+ to the already introduced $\frac{1}{F}i_{veh}$ and j_{veh} with

$$\frac{1}{F}i_{veh} = j_{veh}. \quad (13)$$

The combined flux of ions $\frac{1}{F}i_{veh}$ and the combined backflow j_{veh} are equally convenient for the description of the time evolution of $\Delta c(t)$ outside the steady state. The time evolution of $\Delta c(t)$ with an applied current can be described by a constant term $S = -\text{div}(\frac{1}{F}i_{veh})$, indicating the build up of concentration difference through the applied current, and a time/concentration dependent backflow with constant rate Γ depending on sample volume, thickness of the diaphragm d , and the effective diffusion coefficient through the diaphragm:

$$\frac{d\Delta c}{dt} = S - \Gamma\Delta c(t) \quad (14)$$

With $\Delta c_{t=0} = 0$ the solution to that equation 14 is

$$\Delta c(t) = \frac{S}{\Gamma} (1 - \exp(-\Gamma t)) \quad (15)$$

which runs into a steady state for which j_{veh} and $\frac{1}{F}i_{veh}$ compensate each other (see above) and

$$\Delta c_{steady} = \frac{S}{\Gamma}. \quad (16)$$

Therefore S and i_{veh} can be calculated from the steady state concentration Δc_{steady} and the back flow rate Γ .

The relaxation rate Γ was obtained from the time evolution after turning of the current. For this case j_{veh} cause a relaxation of the the concentration difference (see figure 5 c)

$$\Delta c(t) = \Delta c_{steady} \exp(-\Gamma t). \quad (17)$$

Though this value can theoretically also be obtained from the increase of Δc under applied current, due to the way Δc is measured this method cannot be used here. To measure Δc the cell needs to be taken out of the desiccator, the current is removed and the electrodes are bare of reactant gas. It takes up to half an hour in which the concentration difference already relaxes to stabilize the current flow after this process. It is thus not possible to correct the increase of Δc for that backflow. By measuring Δc without current applied there are no additional waiting times with unclear state of the system and the results are more accurate.

A least square fit of equation 17 to the experimental data is shown in figure 8 and 10.

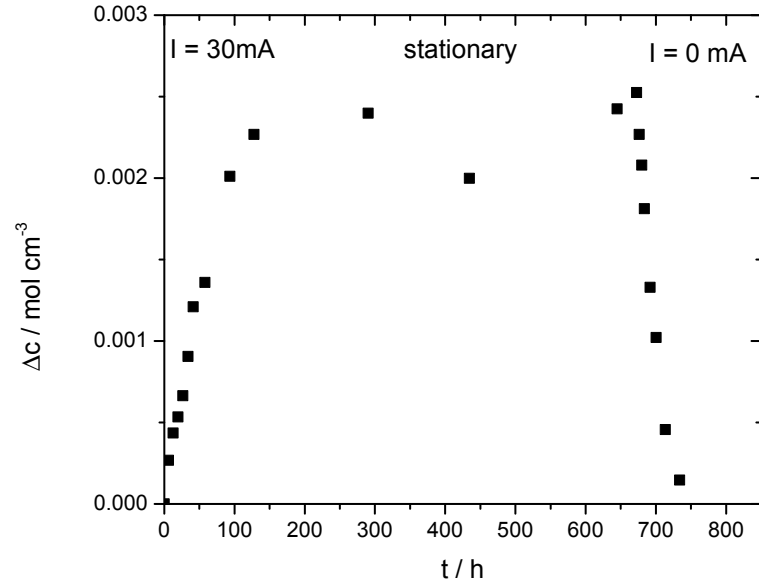


Figure 7: Concentration over time. Starting concentration 85wt%.

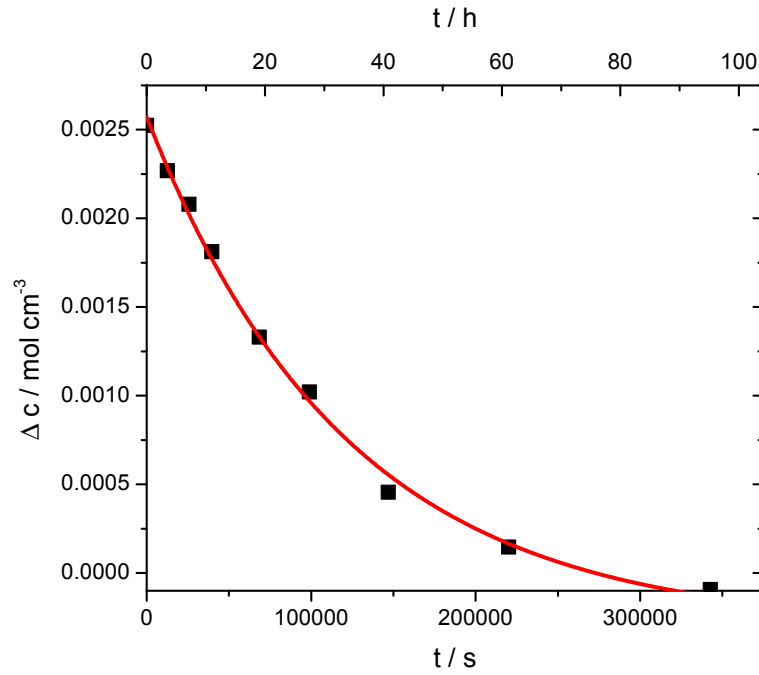


Figure 8: Evolution of Δc over time after turning off the outer current $I_{outer} = 30mA$ and fit of equation 17. Starting concentration 85wt%.

With Γ and Δc_{steady} the transference number t_{veh} is calculated as follows:

$$\Delta c_{steady} \cdot \Gamma = -div \left(\frac{1}{F} i_{veh} \right) \quad (18)$$

$$\int \Delta c_{steady} \cdot \Gamma dx dy dz = \int -div \left(\frac{1}{F} i_{veh} \right) dx dy dz \quad (19)$$

$$\Delta c_{steady} \cdot \Gamma \cdot V = \frac{1}{F} i_{veh} \quad (20)$$

$$i_{veh} = F \Delta c_{steady} \cdot \Gamma \cdot V \quad (21)$$

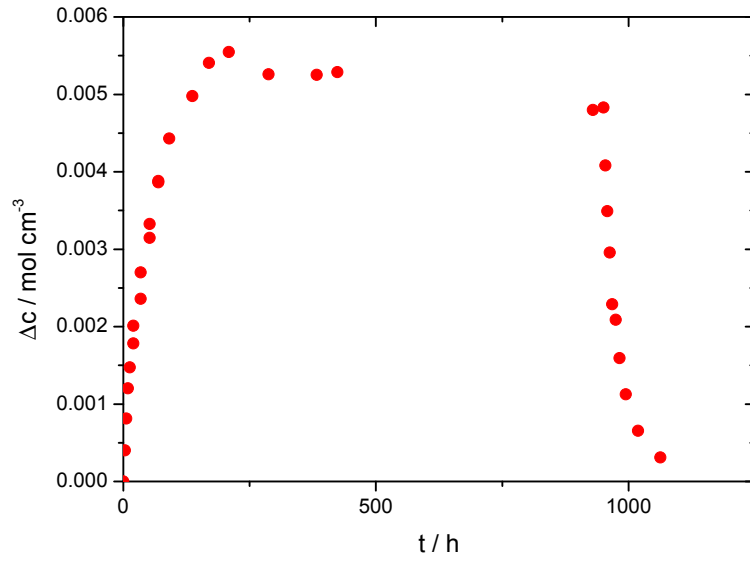


Figure 9: Concentration over time. Starting concentration 73wt%.

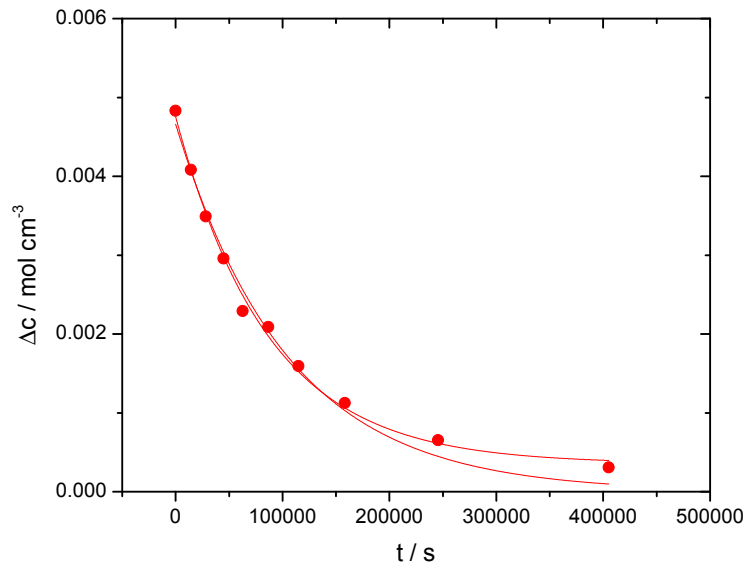


Figure 10: Evolution of Δc over time after turning off the outer current $I_{outer} = 30mA$ and fit of equation 17. Starting concentration 73wt%.

It is:

$$t_{veh} = F \frac{\Delta c_{steady} \cdot \Gamma \cdot V}{I_{outer}} \quad (22)$$

	I_{outer}	Δc_{steady}	Γ	t_{veh}
85wt%	30 mA	0.00288mol/cm ³	$8.22 \cdot 10^{-6}$ 1/s	0.63
73wt%	30 mA	0.00433mol/cm ³	$8.62 \cdot 10^{-6}$ 1/s	0.99
73wt%	30 mA	0.00463mol/cm ³	$6.92 \cdot 10^{-6}$ 1/s	0.85

As the concentration of H_3O^+ and $H_2PO_4^-$ is identical c_{ion} (minor difference at very low water content due to autodissociation of H_3PO_4) the transference numbers $t_{H_3O^+}$ and $t_{H_2PO_4^-}$ ($t_{veh} = t_{H_3O^+} + t_{H_2PO_4^-}$) can be calculated from the ratio of the respective diffusion coefficients $D_{H_3O^+}$ and $D_{H_2PO_4^-}$ as know from PFG-NMR as it is:

$$\sigma_{vehicle} = \frac{F^2}{RT} c_{ion} (D_{H_3O^+} + D_{H_2PO_4^-}). \quad (23)$$

Dissociation constant Dissociation constants are calculated from t_{veh} , the corresponding ion concentrations c_{ion} and the respective concentrations of aqueous (aq) and phosphate (P1) species. In the terminology introduced in the main text and with $[H_3O^+] = [H_2PO_4^-] = [ion]$ the dissociation constant is:

$$K = \frac{[ion]^2}{([aq] - [ion])([P1] - [ion])} \quad (24)$$

The molar ion concentration is therefore:

$$[ion] = \frac{K([aq] + [P1])}{2(K-1)} + \frac{\sqrt{K(K[aq]^2 + 4[aq][P1] - 2K[aq][P1] + K[P1]^2)}}{2(K-1)} \quad (25)$$

Calculations including phosphoric acid's density In calculating $\sigma_{vehicle}^D$ and $\sigma_{structure}^D$ temperature dependent density values for different water contents are used. Summaries of physical properties of H_3PO_4 (aq) can be found in the book of Slack [10], the DOE report of Sarangapani et al. [11], or more recently the article by Korte [12]. Of special importance for this study are the empirical equations for density as a function of temperature and water content. MacDonald and Boyack report an empirical equation; (W = weight percentage of H_3PO_4 (aq); T = Temperature in °C; valid in the range 86-102wt% H_3PO_4 (aq); 25-170 °C):

$$\rho = 0.68235 + 1.20811 \cdot 10^{-2}W - \left(1.2379 \cdot 10^{-3} - 3.7938 \cdot 10^{-6}W\right) T \frac{g}{cm^3} \quad (26)$$

The data of Egan and Luff [13] and Christensen and Reed [14] (15-100wt% H_3PO_4 (aq); 25-60 °C) have been joined and fitted with the following equation:

$$\rho = 0.959185 + 5.42201 \cdot 10^{-3}W + 2.264 \cdot 10^{-5}W^2 + 1.2172 \cdot 10^{-7}W^3 - (2.33111 \cdot 10^{-4} + 4.75028 \cdot 10^{-6}W)T + 2.43866 \cdot 10^{-6}T^2 \frac{g}{cm^3} \quad (27)$$

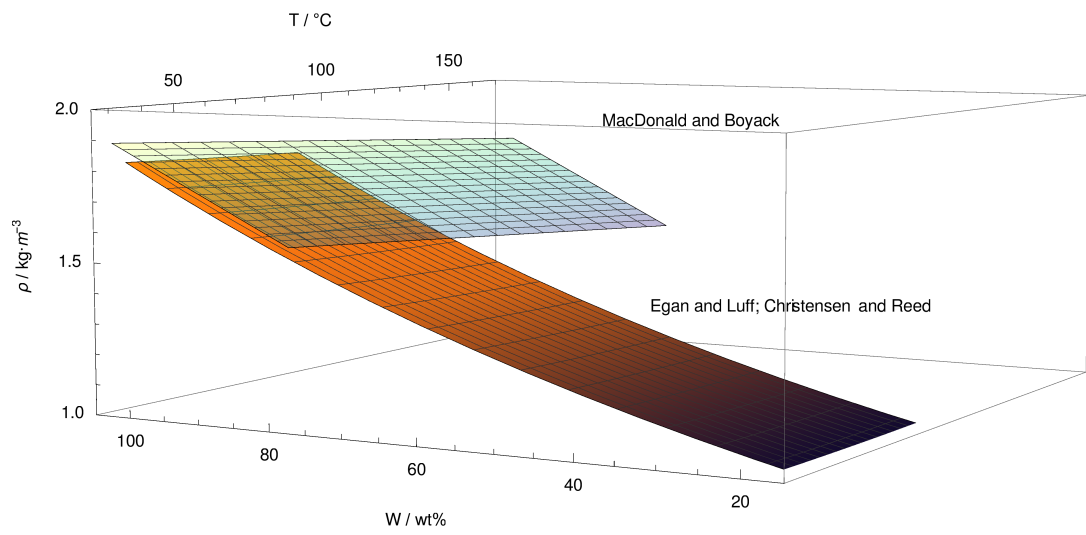


Figure 11: Visualization of empirical density equations by MacDonald and Boyack[15] (blue) and according to data of Egan and Luff [13]; Christensen and Reed [14].

2 Results

2.1 Proton decoupling regime ($\lambda = 2 - 3$)

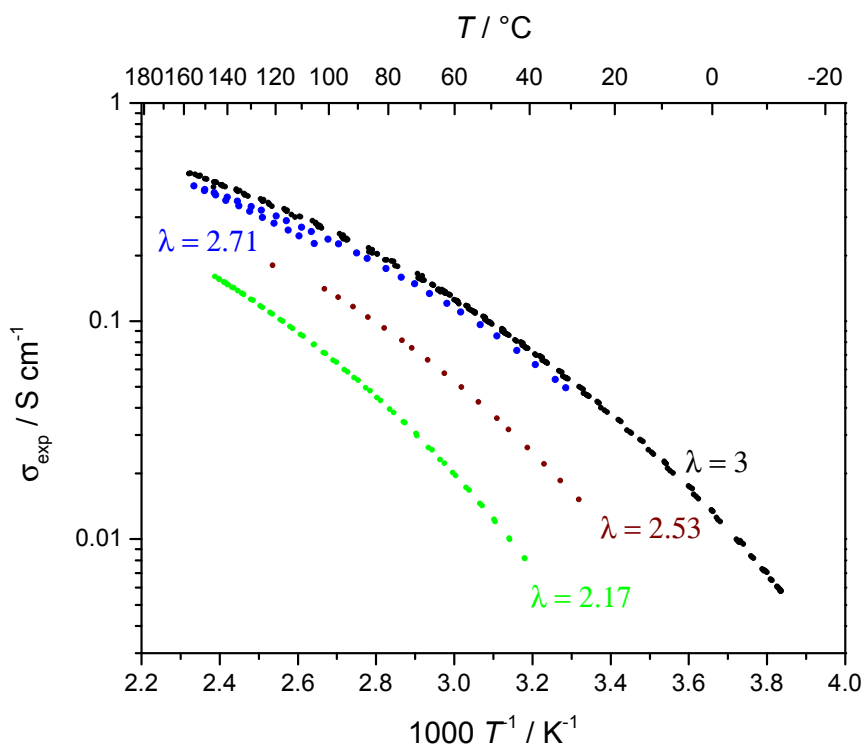


Figure 12: Conductivity measured at different water contents $\lambda < 3$.

2.2 Neat Phosphoric acid ($\lambda = 3$)

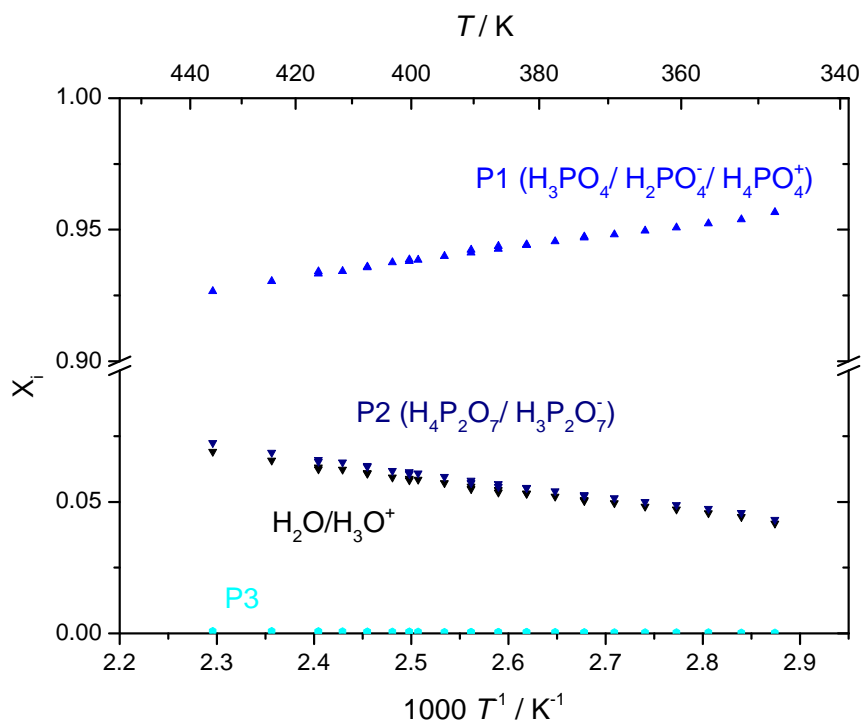


Figure 13: Equilibrium composition in molar fractions of aqueous (H_2O/H_3O^+) and phosphoric acid species for nominally dry phosphoric acid at different temperatures.

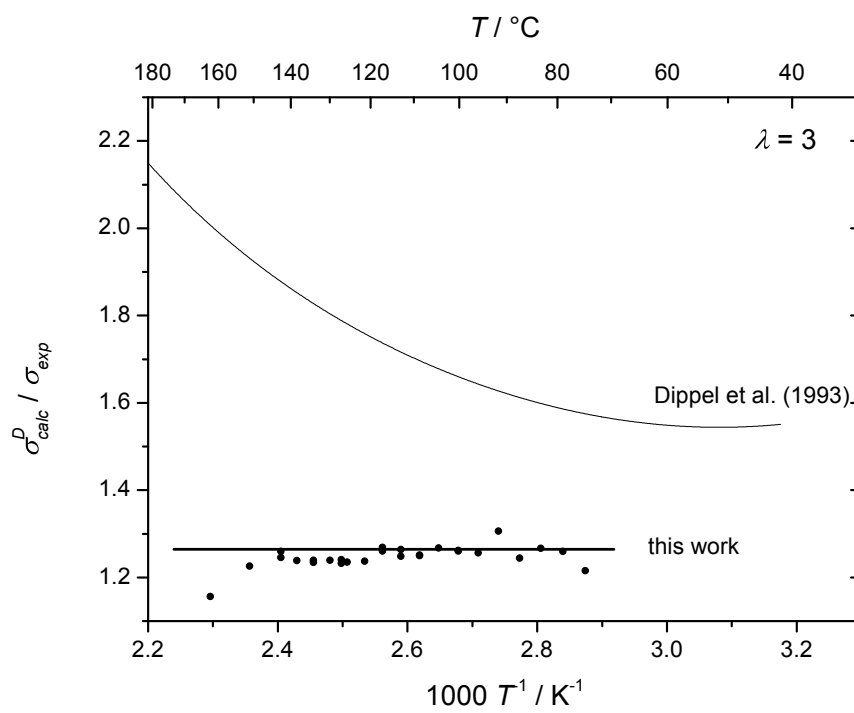


Figure 14: Haven ratio as described in the main text for $\lambda < 3$ in comparison to the data by Dippel et al.[16] for which at the time temperature dependent composition was not available. It turns out that the ratio is constant over the whole investigated temperature regime (see main text).

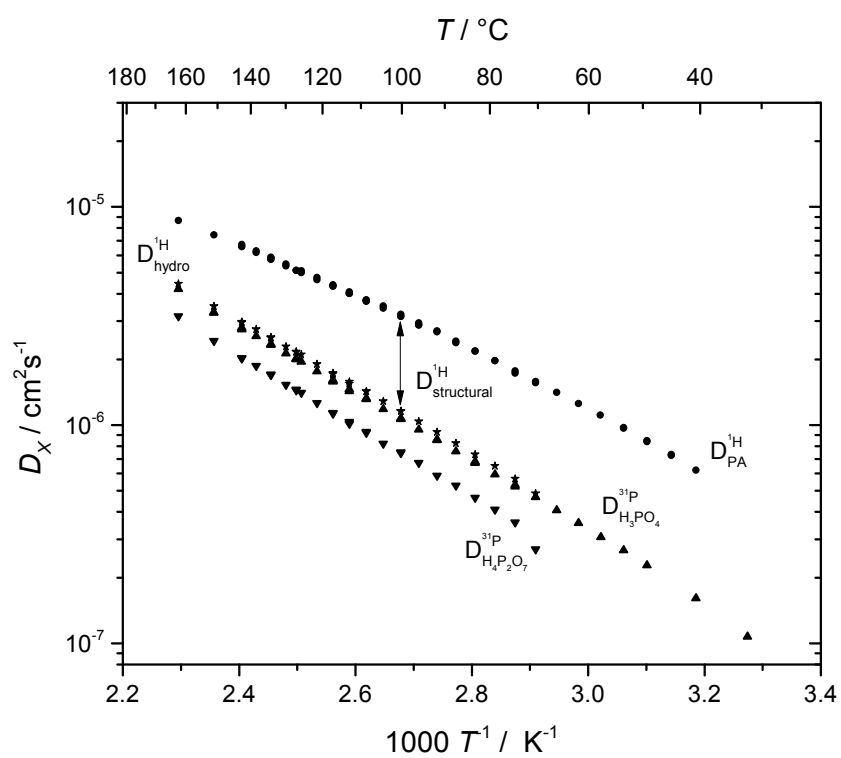


Figure 15: Diffusion coefficient of protons and the phosphate species at $\lambda = 3$.

2.3 Transition regime ($\lambda > 3$)

2.3.1 Transference

The transference $t_{structural} = \frac{\sigma_{structural}}{\sigma_{exp}}$ in the transition regime ($\lambda > 3$) is calculated in the main part of this work. Calculations are based on measured conductivity σ_{exp} and the structural conductivity $\sigma_{structural}$, which is calculated with NMR diffusion data for H_2PO_4^- and H_3O^+ and the concentration of those ions calculated from the dissociation obtained through the transference experiment conducted at $T = 60^\circ\text{C}$. As dissociation is temperature dependent it is not strictly valid to calculate $\sigma_{structural}$ from that data set at other temperatures than $T = 60^\circ\text{C}$. It is important to note, though, that even with non temperature dependent dissociation the trends for the temperature dependence of $t_{structural}$ are valid. Temperature dependence in the raw data is included through the temperature dependent concentration of phosphoric acid and aqueous species (see main text, water concentration increases towards higher temperatures) and $t_{structural}$ decreases with increasing temperature (see figure ??).

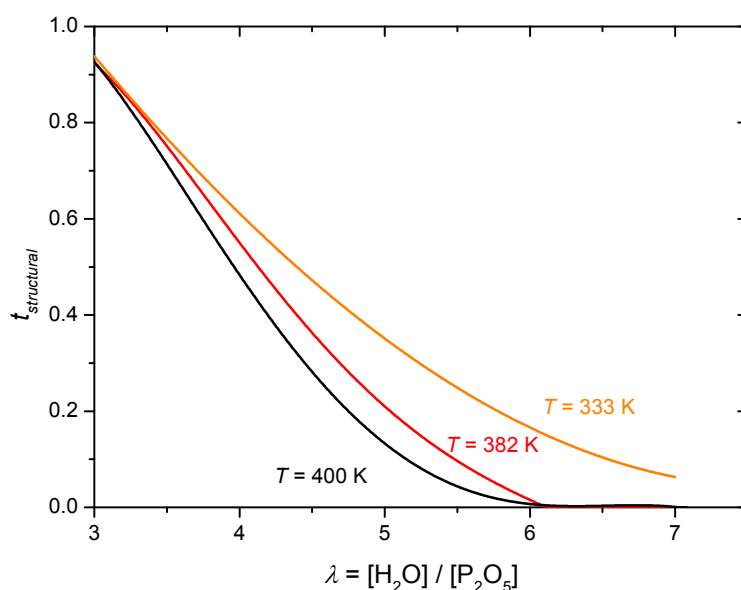


Figure 16: Transference number for structure diffusion at different temperature ($\lambda > 3$). Contributions of ionic species to conductivity have been calculated assuming dissociation of H_3PO_4 according to the dissociation as obtained through the transference experiment at $T = 333\text{K}$. As dissociation is temperature dependent this assumption is not strictly valid, but the trend that transference numbers decrease towards higher temperature are clear.

Additionally a consistency check of the data set presented in figure 16 and in the main text with proton diffusion data obtained purely through PFG-NMR was conducted. While conductivity measurements through AC-impedance only measure the transport of charged species contributing to conductivity, ^1H PFG-NMR measures the diffusion of all protons – the ones contributing to conductivity and the ones that do not contribute. With the high number of diffusing protons not contributing to conductivity and in fact to structural proton diffusion at increasing water contents calculating the conductivity due to structural proton diffusion only from diffusion data is prone to error. Even the structural diffusion coefficient $D_{structural}^{1H} = D^{1H} - D_{hydrodynamic}^{1H}$ cannot be obtained without further assumptions on the concentration of H_2PO_4^- and H_3O^+ . However, we like to point out at the example of $T = 382\text{K}$ for which proton diffusion, diffusion of aqueous species, and diffusion of phosphoric acid species were measured the ratio $D_{structural}^{1H} / D^{1H}$ (see figure 17) is consistent with the decay of $t_{structural}$ at the same temperature.

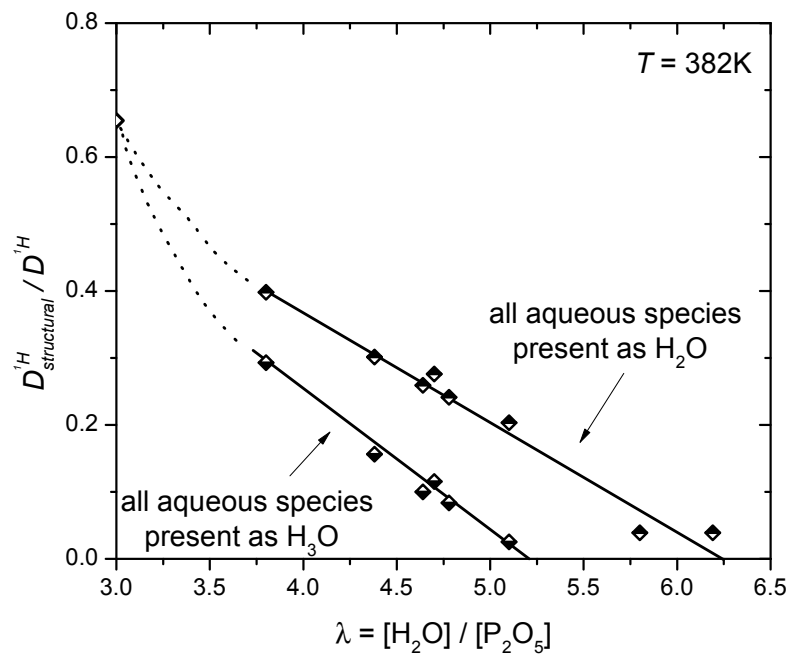


Figure 17: The decay of $D_{structural}^{1H} / D^{1H}$ at increasing water contents as calculated purely from PFG-NMR diffusion data. To obtain $D_{structural}^{1H}$ assumptions on the protonation of the aqueous species need to be made (see main text) and here the limiting cases, viz. all aqueous species being unprotonated (all are present as H_2O) all aqueous species being protonated (all are present as H_3O^+) are shown. The decay of structural diffusion calculated from conductivity data (see figure 16) is within those limits at $T = 382\text{K}$.

2.3.2 Dissociation

Calculation of vehicle conductivity $\sigma_{vehicle}$ from diffusion data through the Nernst-Einstein equation (eq. 23) relies on concentrations of all ions present in the solution. As those concentrations cannot be measured directly (see main text) but have been obtained through the dissociation of H_3PO_4 measured through transference experiment (see above) for two water contents λ , dissociation at different water content λ needed to be interpolated for the calculations in the main text (figure 13 main text). As the dissociation constant α for dissociation of H_3PO_4 does not change monotonically at the investigated water contents the monotonically changing $[H_3O^+][H_2PO_4^-]/[H_2O][H_3PO_4]$ has been interpolated instead and the values are shown in figure 18 with literature data on higher water contents.[17, 18]

Below $\lambda = 5$ the influence of slight changes in $[H_3O^+][H_2PO_4^-]/[H_2O][H_3PO_4]$ on $\sigma_{vehicle}$ is not very large and the constant value obtained at $\lambda = 4.92$ has been used in lack of more accurate dissociation data.

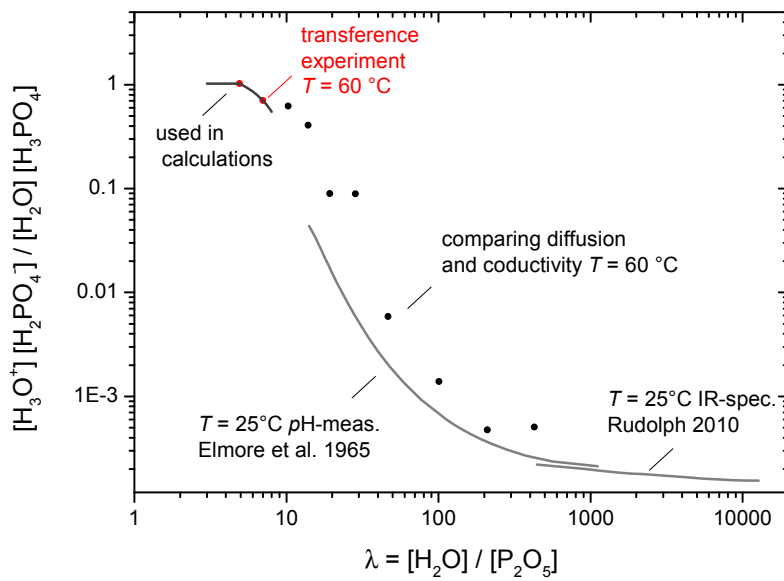


Figure 18: Dissociation $[H_3O^+][H_2PO_4^-]/[H_2O][H_3PO_4]$ at different λ from literature [17, 18] (gray), from transference measurements (red), through comparison of diffusion and conductivity data (black points) and the interpolations used for calculations in the main text (dark gray))

2.3.3 Chemical Shifts

Gerlt et al.[19] have shown that protonation of the phosphate oxygens causes a downfield shift of the ^{17}O resonance. The possibility to obtain information on dissociation by this technique was briefly investigated.

The data presented in figure 19 exhibit almost identical ^{17}O chemical shifts throughout the *acidic aqueous regime* ($\lambda > 11$) and reproduce the ^{17}O chemical shifts reported by Christ et al.[20] and Gerothanassis and Shepard[21]. In the *viscosity controlled regime* ($\lambda < 11$) and at lower λ the phosphate ^{17}O resonance is shielded. The water ^{17}O resonance, on the other hand, is deshielded (with increasing protonation) for all $\lambda < 1000$.

However, at very low λ the low factual water content of the samples does not allow for accurate measurement of the the water ^{17}O resonance and the phosphate ^{17}O resonance scatters considerably. We therefore show and discuss ^{31}P NMR chemical shifts in the main text which show the same trends. The phosphate ^{17}O and ^{31}P resonance both depend on the water concentration and reach a critical transition at approximately $\lambda = 11$ (see main text).

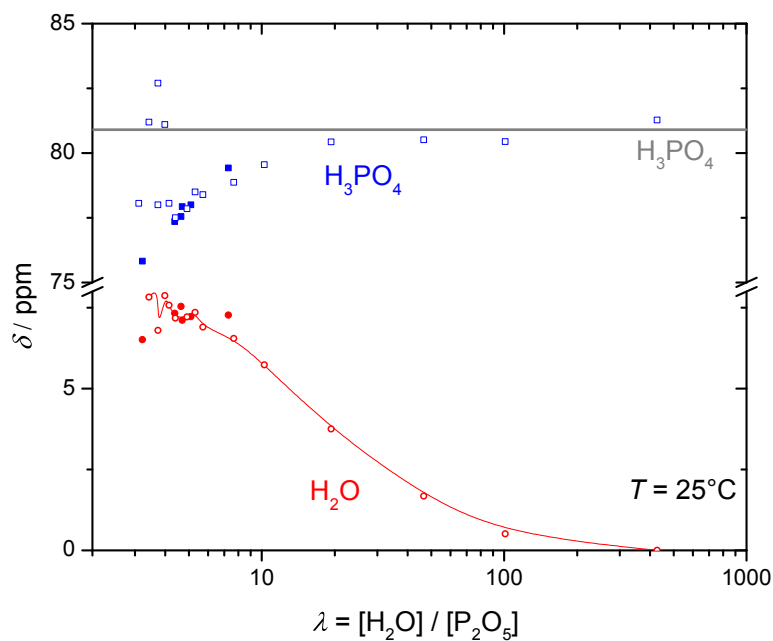


Figure 19: Chemical ^{17}O shifts of the phosphate species and H_2O reference to plain the ^{17}O resonance in distilled water.

2.3.4 Diffusion Coefficients

In the following a selection of diffusion data at different water content λ and temperature T is given including a comparison to literature data in figure 21.

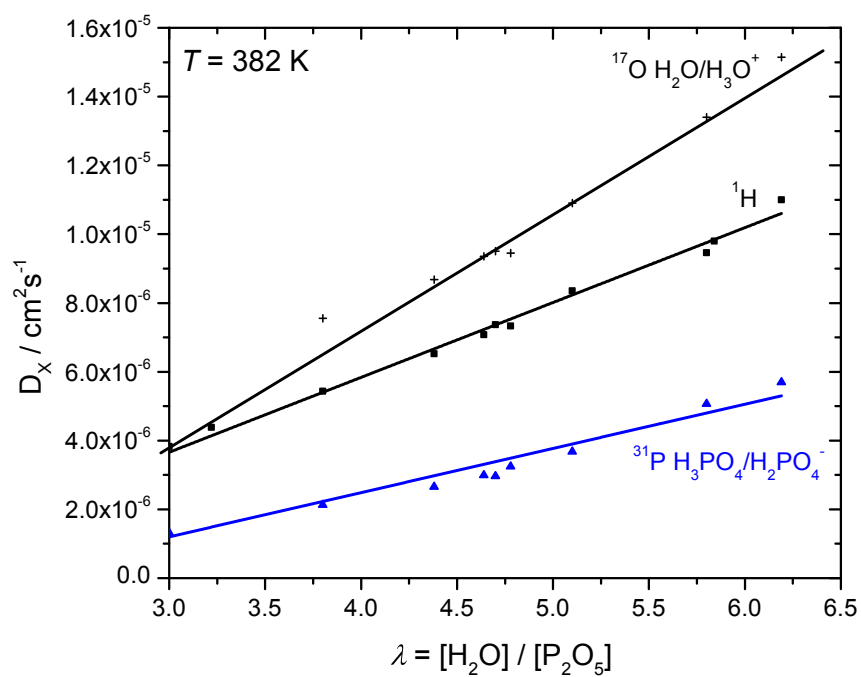


Figure 20: Diffusion coefficients of protons, water and phosphoric acid species at $T = 382 \text{ K}$ ($3 < \lambda < 7$).

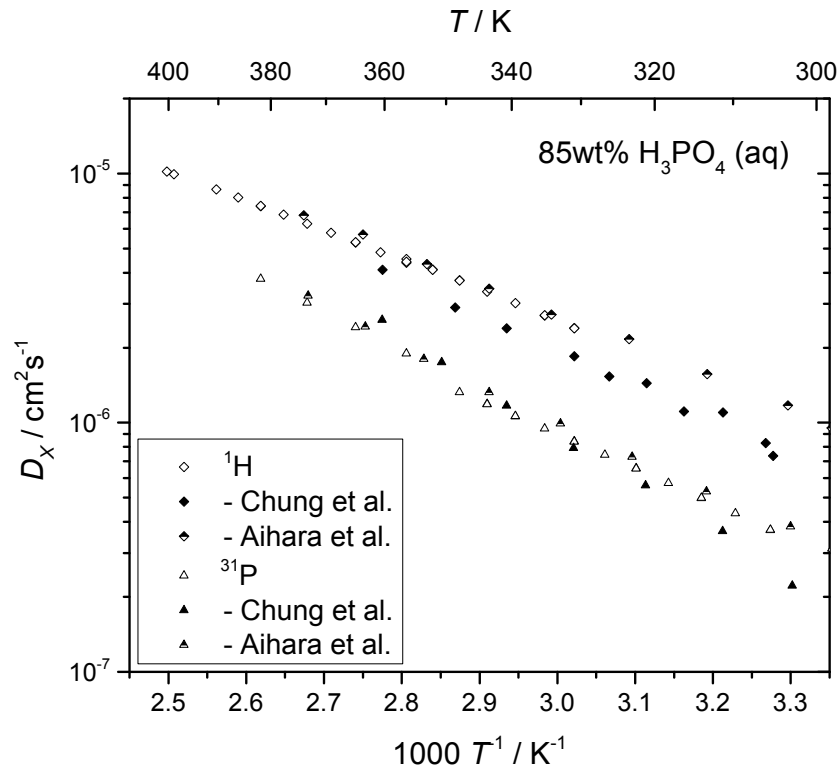


Figure 21: Temperature dependent diffusion coefficients (^1H and ^{31}P at 85wt% H_3PO_4 (aq) ($\text{P}_2\text{O}_5 \cdot 4.92\text{H}_2\text{O}$, $\text{H}_3\text{PO}_4 \cdot 0.96\text{H}_2\text{O}$ in comparison to available literature data by Chung et al.[22] and Aihara et al. [23]

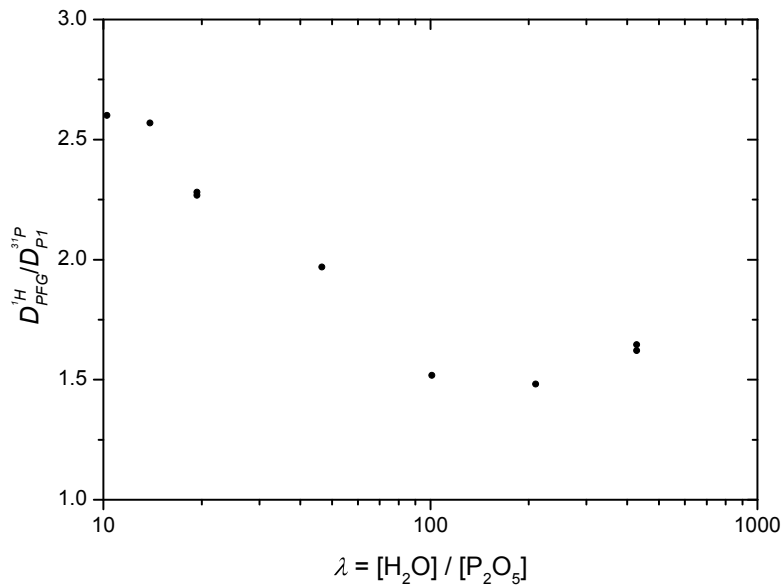


Figure 22: Ratio $D_{\text{PFG}}^{1\text{H}} / D_{\text{P1}}^{31\text{P}}$ for $10 < \lambda < 432$ at $T = 343\text{K}$.

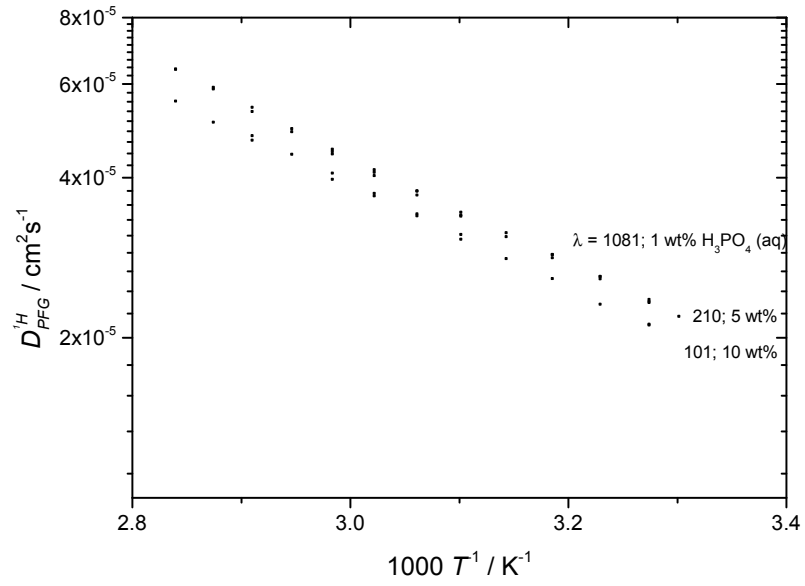


Figure 23: Proton diffusion measured at different water contents $\lambda > 101$.

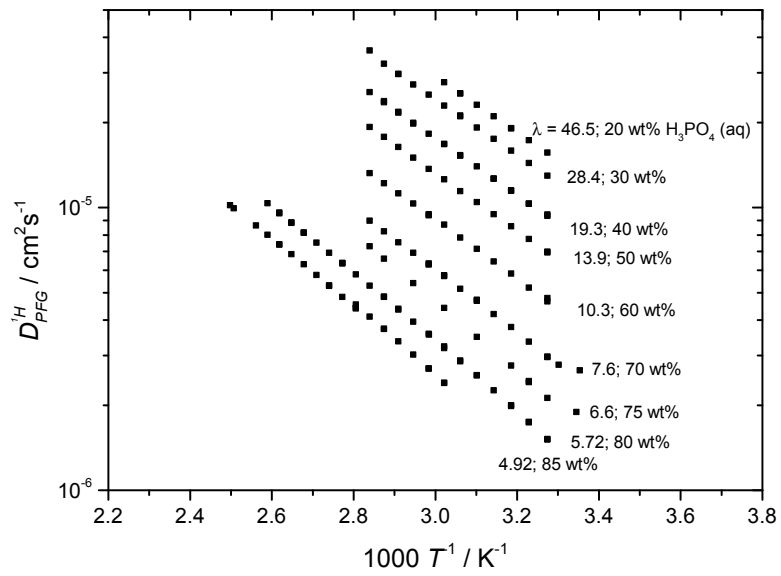


Figure 24: Proton Diffusion measured at different water contents $5 < \lambda < 46.5$.

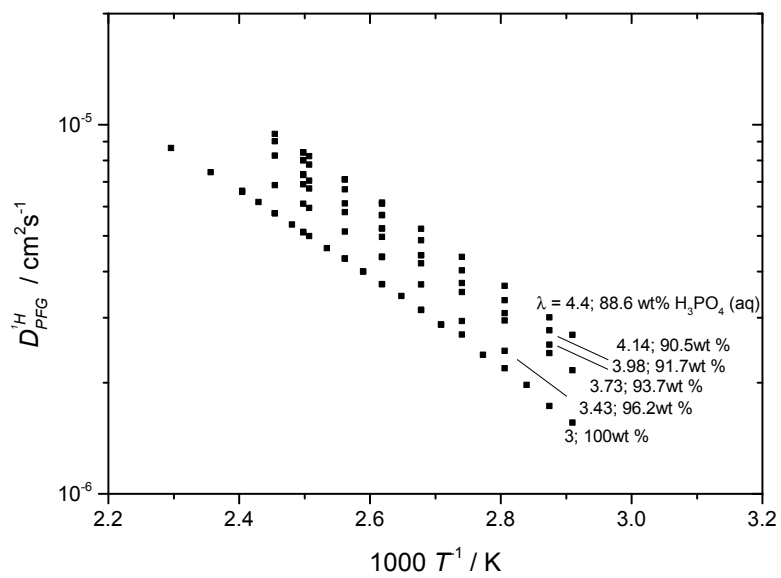


Figure 25: Proton Diffusion measured at different water contents $3 < \lambda < 4.4$.

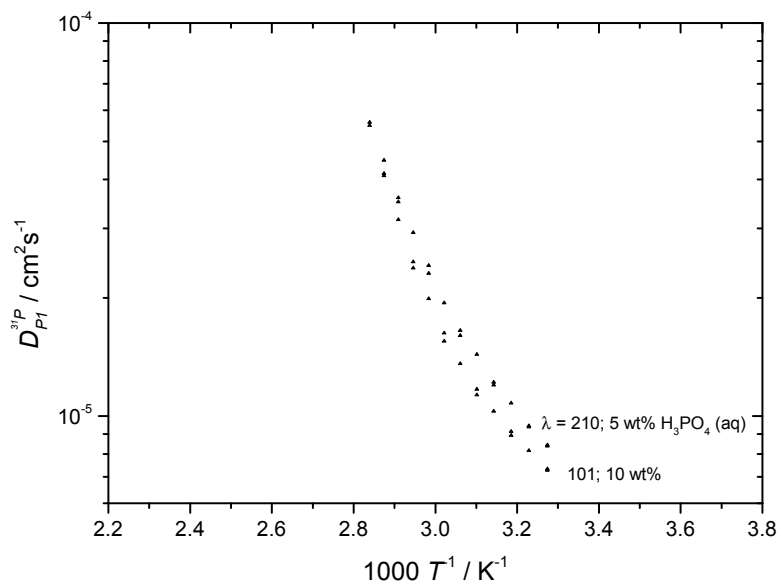


Figure 26: Phosphorous diffusion measured at different water contents $\lambda > 101$.

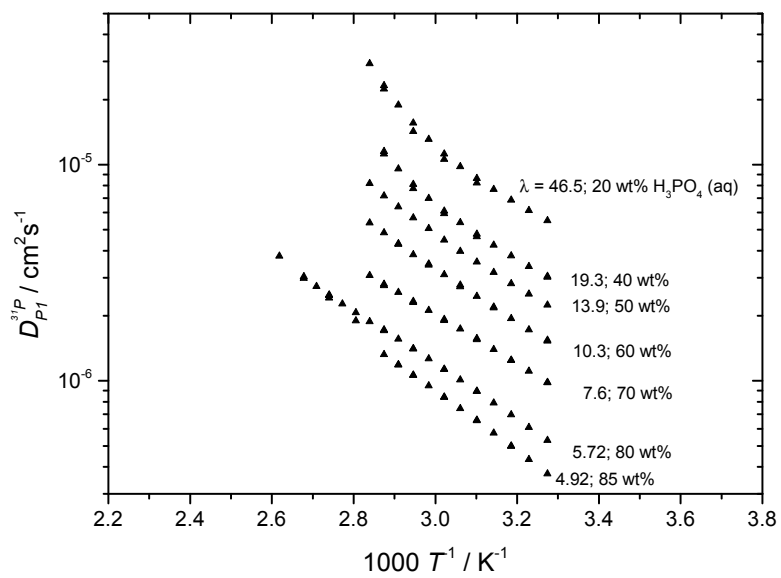


Figure 27: Phosphorous diffusion measured at different water contents $5 < \lambda < 46.5$.

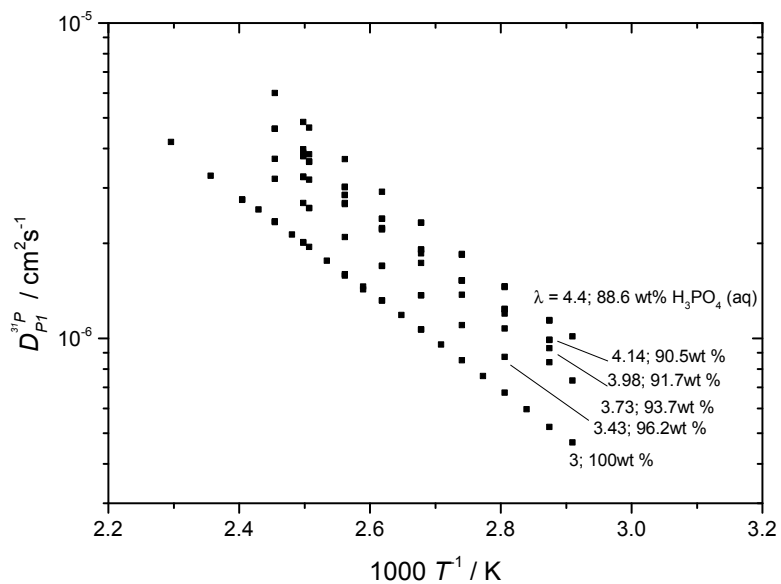


Figure 28: Phosphorous diffusion measured at different water contents $3 < \lambda < 4.4$.

2.3.5 Conductivity

In the following a selection of conductivity data at different water content λ and temperature T is given.

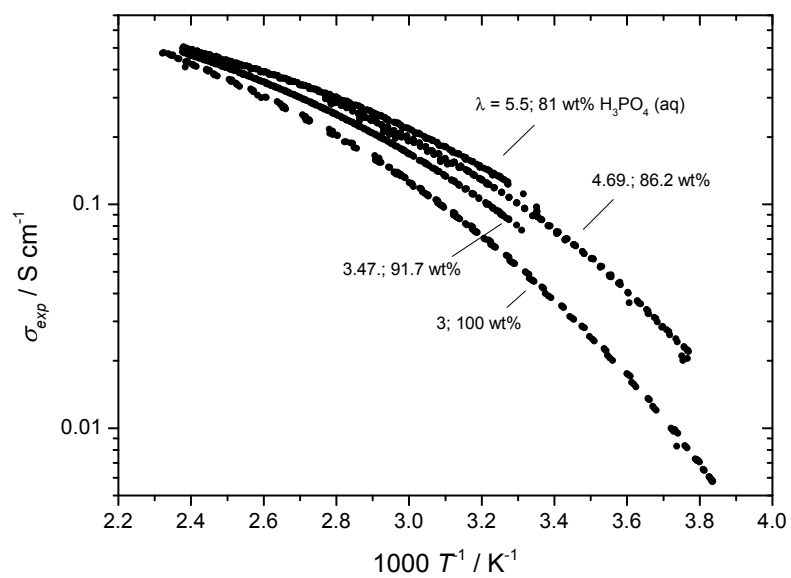


Figure 29: Conductivity measured at different water contents $3 < \lambda < 5.6$.

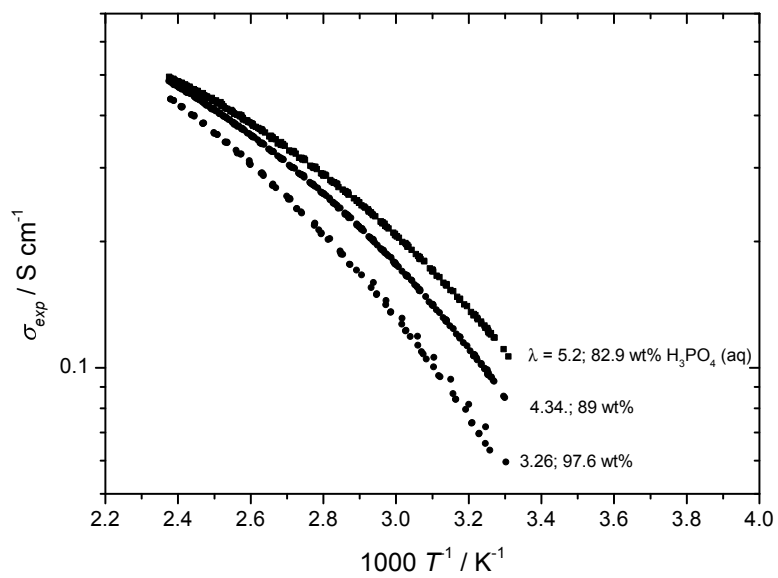


Figure 30: Conductivity measured at different water contents $3.47 < \lambda < 5.2$.

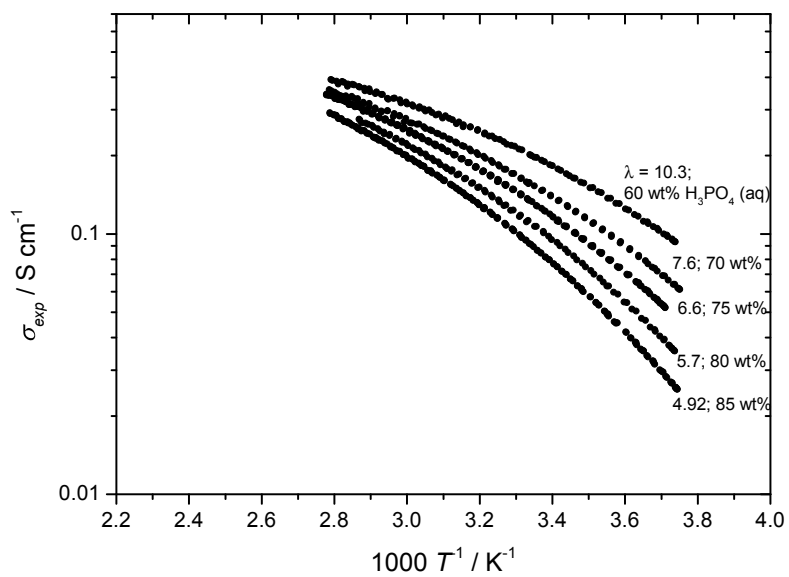


Figure 31: Conductivity measured at different water contents $4.92 < \lambda < 13$.

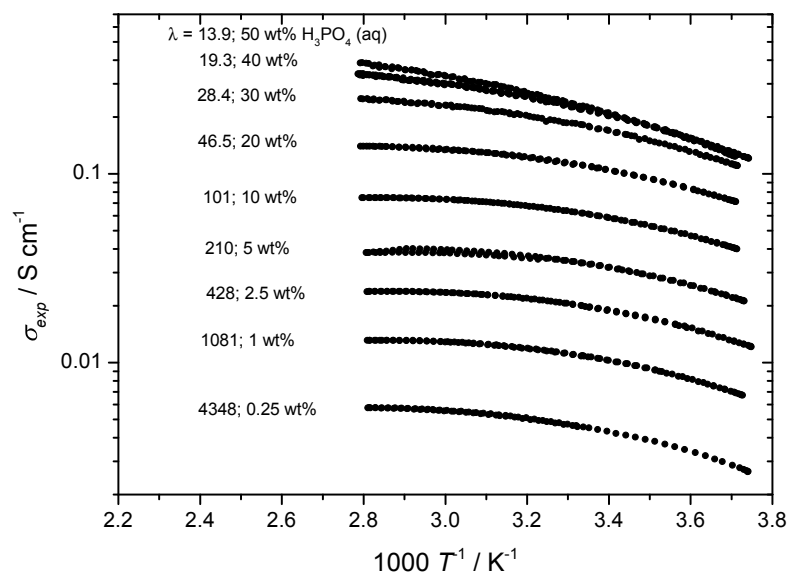


Figure 32: Conductivity measured at different water contents $\lambda > 13$.

References

- [1] D. Lide, ed. *CRC Handbook of Chemistry and Physics*. 90th. CRC Press: Boca Raton, FL, 2009.
- [2] R. A. Munson. "Self-Dissociative Equilibria in Molten Phosphoric Acid". In: *The Journal of Physical Chemistry* 68.11 (1964), pp. 3374–3377. DOI: 10.1021/j100793a045.
- [3] A.-L. Huhti and P. A. Gartaganis. "The composition of the strong phosphoric acids". English. In: *Canadian Journal of Chemistry-Revue Canadienne de Chimie* 34.6 (1956), 785–797. DOI: 10.1139/v56-102.
- [4] R. Jameson. "The composition of the strong phosphoric acids". English. In: *Journal of the Chemical Society FEB* (1959), 752–759. DOI: {10.1039/jr9590000752}.
- [5] O. K. Kudra, Y. Y. Fialkov, and A. N. Zhitominskii. In: *Russ. J. Inorg. Chem.* 9 (1964), p. 1324.
- [6] M. Selvaratnam and M. Spiro. In: *Trans. Faraday Soc.* 61 (1964), p. 360.
- [7] M. Kerker, H. E. Bowman, and E. Matijevic. In: *Trans. Faraday Soc.* 56 (1960), p. 1039.
- [8] E. O. Schmalz. "Bestimmung der Dampfdruckkurven von Wasser über Phosphorsäure". In: *Zeitschrift für Physikalische Chemie* 245 (1970), pp. 344–350.
- [9] A. Wexler and S. Hasegawa. "Relative Humidity-Temperature Relationships of Some Saturated Salt Solutions in the Temperature Range 0 to 50°C". In: *Journal of Research of the National Bureau of Standards* 53 (1954), pp. 19–25.
- [10] A. V. Slack, ed. *Phosphoric Acid*. Fertilizer science and technology series. M. Dekker, New York, 1968.
- [11] S. Sarangapani, P. Bindra, and E. Yeager. *Physical and Chemical Properties of Phosphoric Acid*. DOE Final Report. U.S. Department of Energy.
- [12] C. Korte. "Phosphoric Acid, an Electrolyte for Fuel Cells – Temperature and Composition Dependence of Vapor Pressure and Proton Conductivity". In: *Fuel Cells Science and Engineering - Materials, Processes, Systems and Technologies*. Ed. by B. Emonts and D. Stolten. Vol. 1. Wiley, Apr. 2012. Chap. 9, pp. 335–359.
- [13] E. Egan and B. Luff. "Density of aqueous solutions of phosphoric acid - measurements at 15-degrees-C to 80-degrees-C". In: *Industrial and engineering chemistry* 47.6 (1955), pp. 1280–1281. DOI: 10.1021/ie50546a062.
- [14] J. H. Christensen and R. B. Reed. "Design and analysis data density of aqueous solutions of phosphoric acid - measurements at 25-degrees-C". In: *Industrial and engineering chemistry* 47.6 (1955), pp. 1277–1280. DOI: 10.1021/ie50546a061.
- [15] D. MacDonald and J. Boyack. "Density, electrical conductivity, and vapor pressure of concentrated phosphoric acid". In: *Journal of Chemical and Engineering Data* 14.3 (1969), p. 380. DOI: 10.1021/je60042a013.
- [16] T. Dippel et al. "Proton conductivity in fused phosphoric acid; A $^1\text{H}/^{31}\text{P}$ PFG-NMR and QNS study". In: *Solid State Ionics* 61.1-3 (1993), pp. 41–46. DOI: 10.1016/0167-2738(93)90332-w.
- [17] K. L. Elmore et al. "Dissociation of Phosphoric Acid Solutions at 25°C". In: *The Journal of Physical Chemistry* 69.10 (1965), pp. 3520–3525. DOI: 10.1021/j100894a045.
- [18] W. Rudolph. "Raman-Spectroscopic Measurements of the First Dissociation Constant of Aqueous Phosphoric Acid Solution from 5 to 301 °C". In: *Journal of Solution Chemistry* 41.4 (2012), pp. 630–645. DOI: 10.1007/s10953-012-9825-4.
- [19] J. A. Gerlt, P. C. Demou, and S. Mehdi. "Oxygen-17 NMR spectral properties of simple phosphate esters and adenine nucleotides". In: *Journal of the American Chemical Society* 104.10 (1982), pp. 2848–2856. DOI: 10.1021/ja00374a026.
- [20] H. A. Christ et al. "Chemische Verschiebungen in der kernmagnetischen Resonanz von ^{17}O in organischen Verbindungen". In: *Helvetica Chimica Acta* 44.3 (1961), pp. 865–880. DOI: 10.1002/hlca.19610440331.

- [21] I. P. Gerothanassis and N. Sheppard. “Natural-abundance ^{17}O NMR spectra of some inorganic and biologically important phosphates”. In: *Journal of Magnetic Resonance (1969)* 46.3 (1982), pp. 423–439. DOI: 10.1016/0022-2364(82)90094-4.
- [22] S. Chung, S. Bajue, and S. Greenbaum. “Mass transport of phosphoric acid in water: A ^1H and ^{31}P pulsed gradient spin-echo nuclear magnetic resonance study”. In: *Journal of Chemical Physics* 112.19 (2000), 8515–8521. DOI: 10.1063/1.481454.
- [23] Y. Aihara et al. “Ion Conduction Mechanisms and Thermal Properties of Hydrated and Anhydrous Phosphoric Acids Studied with ^1H , ^2H , and ^{31}P NMR”. In: *The Journal of Physical Chemistry B* 110.49 (2006), pp. 24999–25006. DOI: 10.1021/jp0644452v.